



Water-assisted selective hydrodeoxygenation of phenol to benzene over Ru composite catalyst in biphasic process†

Cheng Zhang,^{a,c} Chuhua Jia,^c Yang Cao,^a Yao Yao,^c Shaoqu Xie,^c Shicheng Zhang,^{a,b*} and Hongfei Lin^{c*}

Received 00th January 20xx,
Accepted 00th January 20xx

DOI: 10.1039/x0xx00000x

www.rsc.org/

Aromatic hydrocarbons as a liquid fuel have unique combustion properties (high volume energy density, etc.). Thus preserving the aromatic rings while selectively cleaving the C–O bonds in the hydrodeoxygenation of lignin derived substituted phenols without additional consumption of H₂ is of crucial importance. In this regard, the hybridization of niobium oxide with MC (micro-mesoporous carbon) as the support was prepared by the incipient wetness impregnation method and characterized by various techniques, including XRD, SEM, TEM, BET, NH₃-TPD and XPS, etc. Under the mild conditions (200–250 °C and 2.0–10 bar H₂), the Ru/Nb₂O₅-MC catalyst was proved to be highly effective for the hydrodeoxygenation (HDO) of phenol. With regard to achieving a high selectivity to benzene, the biphasic catalytic process in the decalin/water mixed solvent was superior to the monophasic processes in either the decalin or water solvent under the same conditions. Water acted as a co-solvent that prevented the occurrence of side reactions and promoted the catalytic C–O bond scission of phenol. The synergistic effect of the biphasic solvents (decalin and water) and the Ru/Nb₂O₅-MC composite catalysts, which might stabilize the emulsions and decrease the activation energy of HDO, was investigated. Meanwhile, other probe reactions were conducted to elucidate the mechanism of the HDO of phenol. The application of the efficient biphasic catalytic process may provide a promising approach for improving lignin valorization.

1. Introduction

Thermochemical processes, such as pyrolysis, are the prevailing methods of converting lignocellulosic biomass, which is the abundant renewable carbon resources, to biofuels and chemicals. In such a process, raw biomass is directly converted to crude bio-oils, which, unfortunately, have a high oxygen content (30–50 wt.%) as well as some significant disadvantages, such as high acid content, viscosity, corrosion, chemical instability and low heating value.^{1–3} Thus, bio-oils require upgrading to fungible fuels or high value chemicals through partial or complete removal of oxygen. One attractive upgrading option is hydro-treating, i.e. catalytic hydrodeoxygenation (HDO).^{4,5} The complex chemical structure of lignocellulosic biomass leads to hundreds of oxygenated bio-oil compounds, among which phenol and substituted phenols derived from lignin are the precursors of synthesizing aromatic compounds such as benzene, toluene, and xylene (BTX).^{6–8}

Thus, phenol is often chosen as a model compound of lignin-derived phenolics because it contains the C_{aromatic}–OH,⁹ one of the major oxygen-containing functional groups found in lignin-derived

compounds. HDO of phenol has been reported to proceed via two generalized pathways, DDO and HYD.^{10–12} One pathway proceeds through direct deoxygenation (DDO) in which the C–O bond in phenol is directly cleaved to form benzene. The DDO utilizes one hydrogen equivalent for reduction of one phenol molecule. Another pathway is catalytic hydrogenation (HYD) of phenol to cyclohexane, which consumes four hydrogen equivalents for deoxygenation. Although the conversion of phenol into cyclohexane through deep HDO reaction is technically feasible, it carries the penalty of additional H₂ consumption. Indeed, it is highly challenging to selectively cleave the strong aryl ether C–O bond in phenol (414 kJ·mol⁻¹) while preserving the aromatic rings.¹³ Severe process conditions are typically required for HDO of phenolic compounds to synthesize aromatic products in monophasic solvent at high reaction temperatures (~400 °C), which facilitates phenolic C–O bond cleavage, and with high hydrogen pressures (~30 MPa), which alleviates catalyst deactivation by reducing coke formation.^{2,14} Moreover, there is a well-known competition between the hydrogenolysis of C–O bonds and the hydrogenation of the aromatic rings during the HDO of phenol.^{15–17}

The full realization of the bio-refinery concept hinges on the development of highly active and selective catalysts.¹⁸ Therefore, design of new functional catalysts with unique selectivity is the key to overcome the barrier. Several alternatives to traditional catalysts, including noble metal catalysts,^{2,5,11,19,20} metal phosphides,^{21,22} carbides,^{21,23} and nitrides,^{21,24} have been widely recognized, showing differences in removing oxygen from phenolic model compounds. Recently, niobium and titanium-based catalysts have shown great promise in promoting the cleavage of C–O bonds.^{9,10,25,26} Moreover,

^a Shanghai Key Laboratory of Atmospheric Particle Pollution and Prevention (LAP3), Department of Environmental Science and Engineering, Fudan University, Shanghai 200438, China. E-mail: zhangsc@fudan.edu.cn

^b Shanghai Institute of Pollution Control and Ecological Security, Shanghai 200092, China

^c The Gene and Linda Voiland School of Chemical Engineering and Bioengineering, Washington State University, Pullman, WA 99164, USA. E-mail: hongfei.lin@wsu.edu

† Electronic Supplementary Information (ESI) available: BET for 5Nb₂O₅-5MC support and Ru/5Nb₂O₅-5MC catalyst, XPS spectra in the Nb 3d and colour photograph of the emulsion, additional figures and tables. See DOI: 10.1039/x0xx00000x

Ru-based catalysts with particle sizes of ~ 2 nm showed the high activity and DDO selectivity.^{10,26,27} It is reported that the effect of ruthenium metal and acid supports under working conditions is crucial for manipulating the competition steps of DDO and HYD. As H concentration decreases (or low hydrogen pressure) at high temperatures, a disparity in the strength of the adsorbed H species, which are nearby the benzene rings and oxygen atoms, leads to hydrogenolysis of the C–O bond of aryl ethers.^{28–30} The phenolic OH is replaced with H to form benzene by a direct deoxygenation (DDO) pathway.^{10,26} In addition, phenol can also be dehydroxylated to benzene through hydrogenation of phenol to cyclohexanol, dehydration of cyclohexanol to cyclohexene, and dehydrogenation of cyclohexene to benzene.^{31,32}

On the other hand, the approaches of process intensification such as in-situ separation are also promising to increase the selectivity. Many researchers have attempted to couple biphasic reaction/separation system for high conversion and selectivity. In biphasic catalysis, Pickering emulsions stabilized by solid catalyst particles provide a platform for catalyzing interfacial reactions, increasing the contact surface area, and separating the product from the system efficiently.^{33–35} Besides, the wettability of the particles plays a significant role in the emulsion states (water in oil or oil in water) and the catalytic performance.^{36–38} In such a biphasic system, organic solvent extracts hydrophobic intermediates and products and thus significantly impacts on the product distribution and selectivity. For instance, HDO of lignin-derived model compounds (vanillin, guaiacol, eugenol, catechol, etc.) in the biphasic system achieved higher yields of hydrocarbon products than that in the monophasic system.^{33,39–41} Recently, our group has developed a novel biphasic tandem catalytic process (biTCP), in which the hydrophilic and hydrophobic catalysts were partitioned into the aqueous and organic phases, respectively, for the conversion of terpenoids to cycloalkanes.^{42,43} We further demonstrated that that highly hydrophilic carbohydrates (i.e., fructose) can be selectively converted into value-added hydrophobic furan derivative chemicals in the “one-pot” biphasic tandem catalytic process.⁴⁴ In our previous research, we observed that both the selectivity and the kinetic rate in the biphasic tandem catalytic process were significantly higher than those in the monophasic processes. Therefore, we conceive that biphasic catalytic process is a generalized “one-pot” synthesis approach to produce hydrophobic biofuels or bio-based chemicals from relatively hydrophilic biomass feedstock.

In this paper, we are applying the similar approach to develop a biphasic catalytic process for selectively converting phenol to benzene. Here we report our findings on a “one-pot” process of phenol conversion over the Ru/Nb₂O₅-MC catalysts to produce benzene in the biphasic water-decalin solvent. The catalysts were rationally designed with a synergistic effect between the Ru, Nb₂O₅ and MC species that result in the high selectivity to benzene from the conversion of phenol in the biphasic system.

2. Experimental

2.1 Materials

Phenol (> 98%), decalin (> 99%) were purchased from Tokyo Chemical Industry Co. (TCI). Dodecane ($\geq 99\%$), guaiacol (> 98%),

Pluronic P123 ($M_w = 5800$, EO₂₀PO₇₀EO₂₀), Pluronic F127 ($M_w = 12600$, EO₁₀₆PO₇₀EO₁₀₆), niobium chloride (99%), ruthenium acetylacetonate (97%), and fructose were purchased from Sigma-Aldrich. All these chemicals were used without further purification.

2.2 Preparation of catalyst

The mesoporous materials were prepared by using P123 and F127 as the composite template, fructose as the carbon source and niobium chloride as the niobium precursor via a hydrothermal method. Briefly, 0.60 g of P123 and 1.80 g of F127 were dissolved in 40 mL of water, followed by mixing with 1.20 g of niobium chloride and different mass of fructose to get the desired MC/Nb₂O₅ ratios. For instance, when the mass ratio of MC to Nb₂O₅ was 5:5, it was denoted by 5Nb₂O₅-5MC. After stirring for 2 h at room temperature, the solution was transferred into high-pressure reactors and crystallized at 180 °C in the oven for 24 h. Then the solution was filtered and the filter cake was washed with deionized water until reaching the neutral pH value and then was dried at 80 °C overnight. The as-prepared samples were calcined at 700 °C for 3 h under nitrogen atmosphere to obtain the mesoporous niobium oxide-carbon supports finally.

All supported Ru catalysts were prepared by the incipient wetness impregnation method. The composite supports were impregnated with a Ru(acac)₃ solution containing a Ru loading of 1 wt.%. The impregnated samples were then kept overnight for 24 h at room temperature followed with drying at 110 °C for 12 h. Finally, the obtained solid was reduced in a H₂ flow at 200 °C for 3 h prior to use with a heating ramp of 5 °C·min⁻¹.

The Ru content in these catalysts was obtained by inductively coupled plasma atomic emission spectroscopy (ICP-MS). The Ru wt.% of the catalysts was 1 \pm 0.3%.

2.3 Characterization of catalyst

X-ray powder diffraction (XRD) patterns were obtained on a Bruker-AXS D2 PHASER powder X-ray diffractometer using Co-K α radiation source ($\lambda = \text{\AA}$). Measurements were carried out between 10° and 90° at 1°·min⁻¹ and a step size of 0.02° in 2 θ .

The N₂ adsorption isotherms of the CNs were measured at -196 °C using a Quantachrome Autosorb iQ2 instrument. The surface area (S_{BET}) was calculated from the N₂ isotherms by the fitting of Brunauer-Emmett-Teller (BET) method. The total pore volume (V_T) was determined from the amount of N₂ adsorbed at a relative pressure (P/P_0) of ~ 0.99 . The pore size distributions (PSDs) were obtained by Density Functional Theory (DFT) fitting of N₂ adsorption data. The micropore surface area (S_{mic}) was obtained from that pores less than 2 nm in DFT fitting, and microporosity was indicated by the $S_{\text{mic}}/S_{\text{DFT}}$.

X-ray photoelectron spectroscopy (XPS) analyses were performed using a Multilab2000 X-ray photoelectron spectrometer with Mg-K α as the photon source. The binding energies (BEs) reference was taken by using the C 1s peak at 284.6 eV.

The surface properties of the catalysts were investigated by temperature-programmed desorption of ammonia (NH₃-TPD). The samples (50 mg) were reduced at 573 K for 1 h under a flow of H₂ of 60 mL/min and then purged in He flow for 30 min. After reduction, the sample was cooled to 373 K, and the feed composition was switched to a mixture containing 20% NH₃ in He (30 cm³·min⁻¹) for

30 min. The physisorbed ammonia was flushed out with He flow for 1 h. Then, the catalyst was heated at 10 K/min under He to 873 K. The reactor effluent was continuously monitored by mass spectrometry.

The crystal size and morphology of the Nb₂O₅-MC support and the location and size range of the Ru particles were investigated using scanning transmission electron microscopy (STEM), high-resolution transmission electron microscopy (HR-TEM) and energy dispersive X-ray spectroscopy (EDS) analyses. The imaging was performed using a FEI Tecnai F20 field-emission gun with an accelerating voltage of 200 kV. A symmetrical multibeam illumination was used with a Gatan Ultrascan CCD camera, a 30 mrd camera length, and a 1 nm probe size. Data processing and analysis were carried out using the Gatan Digital Micrograph software. Catalyst powder samples were dispersed on lacy carbon copper grids.

The water contact angles were measured at ambient temperature on a self-supporting pressed sample disc by a contact angle meter (Dataphysics, OCA 20). Once a drop of water was deposited on the surface of the sample disc, the contact angle was determined from pictures immediately captured using a charge-coupled-device camera. The water droplets were introduced using a micro syringe, and images were captured to measure the angle of the liquid solid interface; each sample was recorded at three different points.

2.4 Hydrodeoxygenation of phenol

The HDO reactions were carried out in a 45 mL Parr reactor equipped with a magnetic stirrer. In a typical experiment, phenol (0.05 g) and catalyst (0.05 g) were dispersed in a 20 mL mixture of deionized water and decalin. After purging the reactor with hydrogen 6 times, 10 bar of hydrogen was maintained at ambient temperature while stirring at 700 rpm, and then the reactor was heated up to 200 °C. At the end of the reaction period, the reactor was taken apart and cooled to room temperature quickly. To break the emulsion before analysis, the Nano hybrid particles were separated in two steps. In the first one, a common paper filter was used. This coarse paper filter (8-micron pore) trapped a large fraction of the solid particles, which quickly agglomerate over the surface of the filter. In the second step, the two clear liquid phases obtained after filtration were separated and centrifuged at 10000 rpm for 5 min respectively. Then the sample of each phase were analysed by gas chromatography, GC-FID and GC-MS.

The following definitions were used to quantitate experimental datum:

Conversion (%)

$$= [\text{moles of carbon in reactant consumed} / \text{moles of carbon in reactant fed}] \times 100$$

Selectivity (%)

$$= [\text{moles of carbon in the product} / \text{sum of moles of carbon in all products}] \times 100$$

Yield (%)

$$= \text{Conversion} (\%) \times \text{Selectivity} (\%) \div 100$$

3. Results and discussion

3.1 Characterization of the catalysts

3.1.1 BET. The porous texture of these samples was characterized by nitrogen adsorption-desorption at 77 K. The N₂ adsorption-

desorption isotherms are shown in Figure 1A. For MC, 3Nb₂O₅-5MC, 5Nb₂O₅-5MC and 8Nb₂O₅-5MC, the relatively broad knee in the low-pressure range suggests the existence of a significant amount of micropores. Moreover, the Nb₂O₅ support exhibits a type IV isotherm, the typical characteristic of mesoporous materials according to the IUPAC classification.¹² Figure 1B exhibits the pore distribution calculated by the density functional theory (DFT) model. In addition, the porous textural details of these composite materials are summarized in Table 1. Moreover, it can be observed that the specific surface areas of these five supports by both the BET measurement and the DFT calculation decrease as the content of MC decreases gradually. Especially, there are no micropores but only mesoporous ones in the Nb₂O₅ support, which is consistent with the pore distribution of Nb₂O₅ in Figure 1B and Table 1. Moreover, the BET surface area and the total pore volume changed slightly when Ru was loaded onto the 5Nb₂O₅-5MC support, suggesting that Ru nanoparticles (NPs) do not block or alter the pores of the support (Figure S1). Note that the pore size of the 5Nb₂O₅-5MC support is near ~7.0 nm (Table 1).

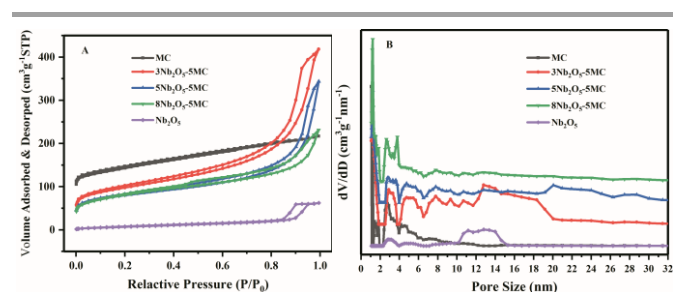


Fig. 1 The nitrogen adsorption-desorption isotherms of five supports (A). The pore size distribution calculated from the adsorption isotherms using DFT method (B)

Table 1 Physical properties of MC, 3Nb₂O₅-5MC, 5Nb₂O₅-5MC, 8Nb₂O₅-5MC, Nb₂O₅ and Ru/5Nb₂O₅-5MC

Catalysts	^a S _{BET} (m ² ·g ⁻¹)	^b S _{micro} (m ² ·g ⁻¹)	^c V _{tatal} (cm ³ ·g ⁻¹)	^d D _p (nm)
MC	523.67	492.77	0.3356	2.56
3Nb ₂ O ₅ -5MC	347.59	184.98	0.6476	7.45
5Nb ₂ O ₅ -5MC	285.42	155.18	0.5314	7.45
8Nb ₂ O ₅ -5MC	287.49	148.09	0.3577	4.98
Nb ₂ O ₅	31.48	0.00	0.0966	12.27
Ru/5Nb ₂ O ₅ -5MC	290.97	136.48	0.5364	7.37

^a Specific surface area calculated by Brunauer-Emmett-Teller (BET) equation.

^b Specific surface area of micro pores calculated by DFT method.

^c The total pore volume was determined from the amount of nitrogen adsorbed at a relative pressure of 0.99.

^d Calculated from the maximum in the BJH pore size distribution.

3.1.2 XRD. The XRD patterns of fresh catalysts obtained using incipient wetness impregnation method are shown in Figure 2. When

the calcination temperature was higher than 650 °C, the orthorhombic Nb₂O₅ phase was formed which is evidenced by the reflection peaks indexed as (001), (180), (181), (002), (380), (212), (202), (2160), (1181), and (382), respectively.^{45,46} Moreover, Figure 2 also showed no X-ray diffraction peaks attributed to the bulk metallic Ru phase probably due to the ultra-finely dispersed small Ru NPs, which was consistent with the HRTEM (Figure 3).

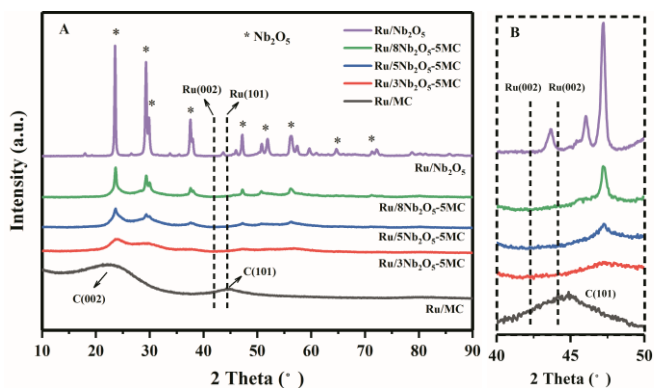


Fig. 2 Powder XRD patterns of the fresh Ru/Nb₂O₅, Ru/Nb₂O₅-MC and Ru/MC catalysts (A). Zoom on Ru (101) and Ru (002) diffraction peak zone from 40 to 50 degree (B).

3.1.3 SEM and TEM. The morphology and microstructures of the Ru/5Nb₂O₅-5MC catalyst was characterized by the scanning electron microscopy (SEM) and transmission electron microscopy (TEM). The SEM images (Figure 3A and 3B) showed the 3D frameworks constituted by the particles with randomly opened micropores, indicating that the pore structures were consistent with the ones observed in the BET results (Figure 1 and Table 1). A typical TEM image, as presented in Figure 3C, indicates that the Ru NPs with a diameter of ~2.5 nm were well distributed on the 5Nb₂O₅-5MC support. Notably, the well-defined crystal lattice fringes are revealed by high-resolution TEM (HRTEM) (Figure 3D), demonstrating apparently distinct morphology profile from the pristine Ru/5Nb₂O₅-5MC hybrid support. Moreover, the Ru NPs have interplanar spacings of 0.205 and 0.234 nm, ascribed to the (101) and (100) crystal planes of Ru, respectively (Figure 3D). Owing to the limitation of resolution, the bright dots of Ru cannot be observed in the HAADF-STEM image of Ru/5Nb₂O₅-5MC, but the EDS mapping proves the existence of highly dispersed Ru species on the 5Nb₂O₅-5MC hybrid support (Figure 3E). The element mapping results further reveal the uniform distribution of Nb, C, and O, confirming the successful hybridization of Nb₂O₅ with MC in the support.

3.1.4 NH₃-TPD. The NH₃-TPD measurements were used to evaluate the strength and distribution of the acid sites on the catalysts. The NH₃ desorption profiles are depicted in Figure S2 and the amount of desorbed NH₃ is compiled in Figure 4. In order to facilitate the analysis, the acid sites are further classified according to their strength. This classification is based on the NH₃ desorption temperature. The acidity distribution was determined by fitting the TPD curves with a Gaussian function and calculating the area corresponding to weak ($T < 250$ °C) and strong (250 °C $< T < 500$ °C)

acidity.^{47,48} The NH₃ desorption peaks below 250 °C correspond to partially ionic NH₄⁺ that are assigned to the weak Brønsted acid sites (BAS), while the NH₃ desorption peaks in the temperature range of 250 to 500 °C are assigned to the strong Brønsted acid sites or the coordinated NH₃ bounded Lewis acid sites (LAS), both of which are considered as the strong acid sites. The areas of the NH₃ desorption peaks which are assigned to the strong acid sites, the weak acid sites and the total acid sites, respectively, are all normalized to the surface area as shown in Figure 4. The NH₃-TPD curves (Figure S2) of all the tested catalyst samples exhibit the similar broad peaks at the temperatures lower than 300 °C, indicating the presence of plentiful weak acid sites on all of the catalysts. Interestingly, compared to the single Nb₂O₅ support, the normalized concentrations of both the weak and the total acid sites on the hybrid Nb₂O₅-MC supports increased substantially, which may explain the better performance of the Ru/Nb₂O₅-MC catalysts.

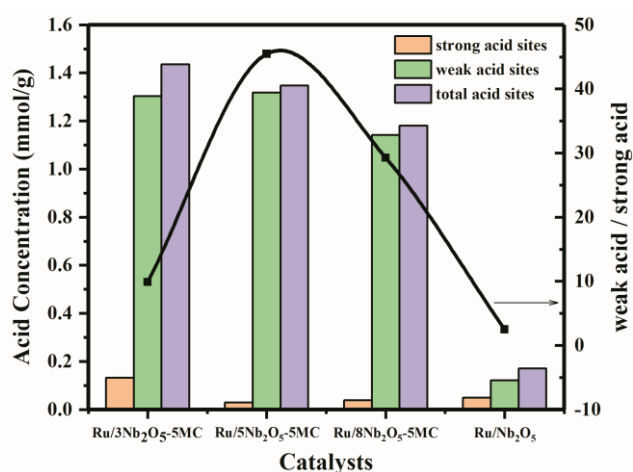


Fig. 4 Acid concentration and the ratio of weak to strong acid of Ru/3Nb₂O₅-5MC, Ru/5Nb₂O₅-5MC, Ru/8Nb₂O₅-5MC and Ru/Nb₂O₅ catalysts.

3.1.5 Wettability. To investigate the wettability of Ru/Nb₂O₅-MC catalysts, the contact angles of water on the surface of the catalysts were measured and the results are shown in Figure S3. The Ru/MC catalyst presents a maximum contact angle of 106°, indicating a very hydrophobic character, while the Ru/Nb₂O₅ catalyst exhibits its good hydrophilicity with near-zero level in contact angle. For the Ru/Nb₂O₅-MC catalysts, as the content of MC decreased, the contact angle gradually decreased, indicating that the surface of the Nb₂O₅-MC composite support became more hydrophilic. In water-oil biphasic solvents, the wettability of the catalyst supports played a key role in forming Pickering emulsions,⁴⁹ with which the desirable catalytic efficiency could be achieved in the water-in-oil system. As expected, the difference in the wettability causes different activity and selectivity of the Ru/Nb₂O₅-MC catalysts. It is found that in aqueous phase reactions, hydrophilic catalysts are more active for the HDO of phenol, because phenol is more soluble in water relative to in decalin. However, in the water-oil biphasic system, the heterogeneity of the catalyst supports with the hybrid hydrophobic MC and hydrophilic Nb₂O₅ domains may compartment the catalyst

at the water-oil interface, and thus stabilize the Pickering emulsions. Moreover, the reactants and intermediates with different hydrophobicity may preferably adsorb on the specific domains of the

composite catalyst, which, therefore, could affect the reaction selectivity.

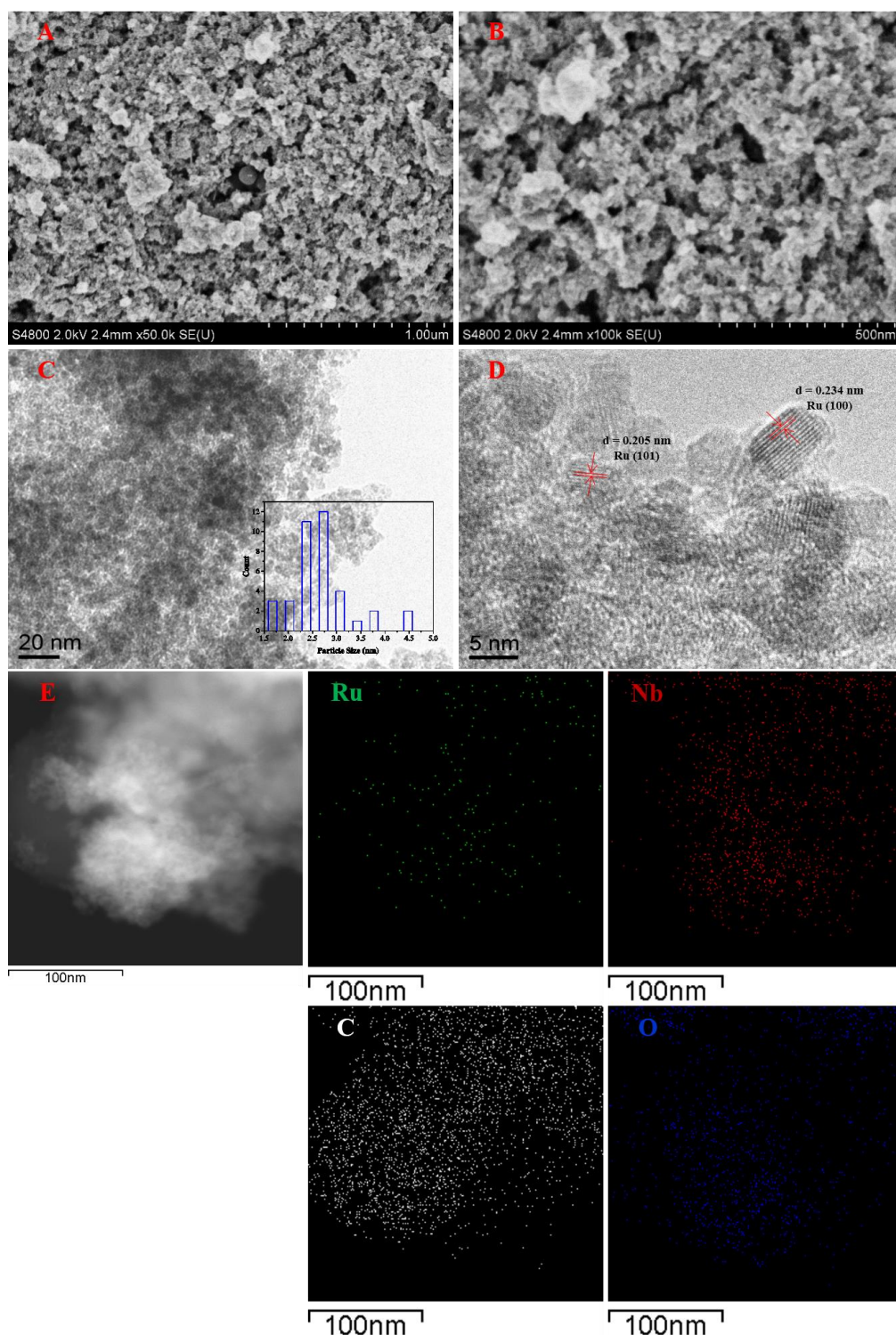


Fig. 3 Representative SEM images (A, B) and TEM images (C, D) of the Ru/5Nb₂O₅-5MC catalyst. Inset (C) the corresponding Ru nanoparticle size distribution histogram. HAADF-STEM image and corresponding EDS elemental mapping images of this hybrid catalyst (E).

3.1.6 XPS. The X-ray photoelectron spectroscopy characterization of Ru in these composite catalysts is shown in Figure 5. The curve

fitting analysis was done in order to resolve multiple Ru oxidative states and to quantify the chemical changes at the growing interface. As seen in Figure 5A, with the C 1s-Ru 3d core level spectra, three different ruthenium chemical states were resolved. The resolved Ru 3d_{3/2} peaks (I, II and III) at binding energy of ~284.3, ~285.2 and ~286.2 eV are originated from the un-reacted/metallic Ru⁰, reacted Ru^{x+} and reacted Ru^{y+} states respectively.^{50–52} The ratio of Ru⁰ / (Ru⁰ + Ru^{x+} + Ru^{y+}) are approximately 27.8%, 39.6%, 40.7%, 36.1%, 39.9% and 38.0% for the fresh Ru/MC, Ru/3Nb₂O₅-5MC, Ru/5Nb₂O₅-5MC, Ru/8Nb₂O₅-5MC, Ru/Nb₂O₅ and the spent Ru/5Nb₂O₅-5MC catalysts, respectively (see Figure 5A and Table S1). The results indicate that there are more metallic Ru nanoparticles and/or nanoclusters on the surface of 5Nb₂O₅-5MC, which is in agreement with the TEM observation (Figure 3C and D). Moreover, in the cases of the other supports, there are more Ru^{x+} or Ru^{y+} ions to interact with Nb₂O₅ to form Ru-O-Nb bonds, and thus a higher percentage of ruthenium oxides would be observed (Table S2 and Figure S4). On the other hand, the O 1s spectra of these Ru catalysts are significantly different (Figure 5B). The peaks 531.2 eV in binding energy can be assigned to lattice oxygen (O²⁻, O_β), while those at 533.1 eV are the characteristic of oxygen vacancies (O/OH, O_α). It is common to evaluate the concentration of oxygen vacancies using the O_α / (O_α+O_β) ratio.^{51,53,54} The highest ratio is 63.0% for Ru/5Nb₂O₅-5MC among these catalysts (Table S3), which suggests that the concentration of oxygen defects on the surface of Ru/5Nb₂O₅-5MC is higher than those on the other catalysts. The Ru oxide peak (O²⁻, O_β) implies that surface oxides are presented on the Ru nanoparticles. Thus, for the as-received Ru catalysts without any reduction pretreatment, the Ru oxides are present in a significant amount.

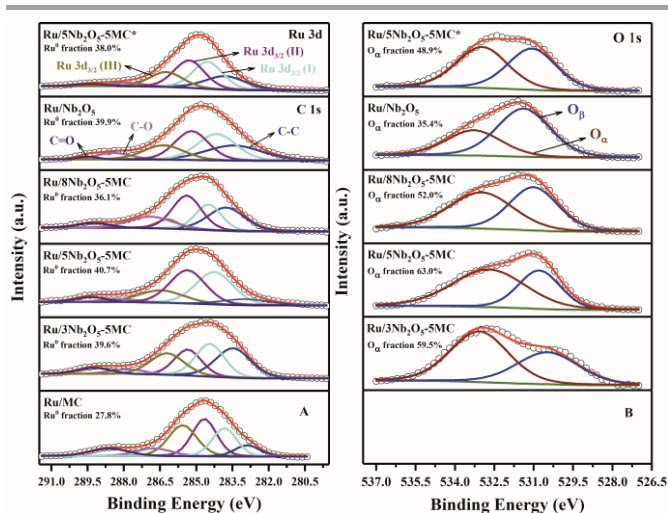


Fig. 5 XPS spectra in the C 1s-Ru 3d (A) and O 1s (B) regions for the fresh and spent (*) catalysts.

3.2 Catalytic activity

3.2.1 Influence of catalyst support and biphasic solvent system.

Catalytic cleavage of aromatic C–O bonds via hydrodeoxygenation (HDO) is known to be challenging, requiring harsh conditions such as high temperatures, high H₂ pressures, strong acids, etc.⁵⁵ Indeed, the phenolic C–O bond energy is large (468 kJ/mol) and makes the direct

hydrogenolysis of C–O bonds more difficult than hydrogenation of arenes, as it typically requires severe conditions that lead to a low selectivity to the desired end product, benzene.⁵⁶ As such, there exist two competing reactions, hydrogenolysis of C–O bonds and hydrogenation of the aromatic rings, during phenol HDO. While there are ample researches on new catalytic materials to improve the selectivity to benzene from the HDO of phenol in a single solvent phase, to the best of our knowledge, there is lack of investigations of new catalytic materials in a biphasic solvent system. Herein, we design the Ru catalysts on the Nb₂O₅-MC (micro/meso-porous carbon) composite supports for the HDO of phenol in the water-decalin biphasic solvent system. Metal oxide nanoparticles have previously been used to stabilize oil-in-water emulsions because their hydrophilicity preferentially orients them toward the aqueous phase at the interface.⁵⁷ In contrast, hydrophobic MC can also stabilize emulsions, but of the water-in-oil variety. Therefore, by tuning the compositions of the hybrid Nb₂O₅-MC composites, we could modify the hydrophilic-hydrophobic balance and assemble water-in-oil or oil-in-water emulsions reproducibly.

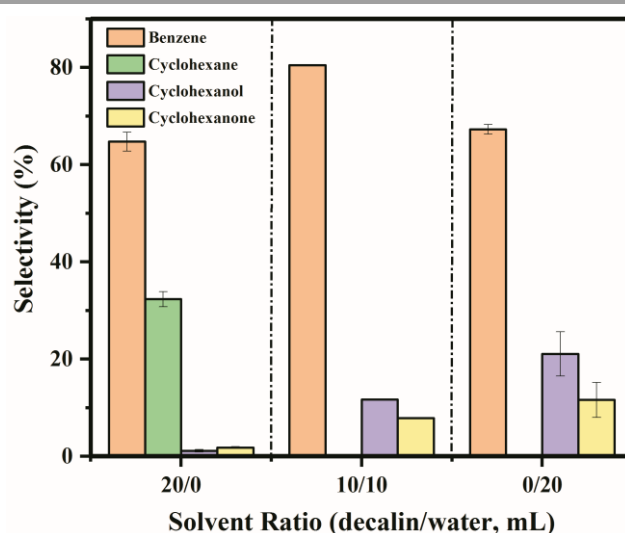


Fig. 6 Selectivity to benzene in HDO of phenol under the biphasic (decalin and water) and monophasic (decalin or water) systems. Conditions: phenol (0.05 g), Ru/5Nb₂O₅-5MC (0.05 g), 250 °C, 2 bar of hydrogen, 4 h.

We demonstrated that the Nb₂O₅-MC composite supported Ru catalyst was active and selective towards to cleaving the C–O bonds in phenol at moderate temperatures with pressurized H₂ in monophasic and biphasic systems. As shown in Figure 6, the selectivity to benzene was ~80% in the biphasic system (decalin and water), while ~65% in the monophasic systems (decalin or water), indicating that benzene was prone to be generated over the Ru/5Nb₂O₅-5MC catalyst under a low hydrogen pressure (2 bar) and at a relatively high temperature (ca. 250 °C). Significantly, the polar and nonpolar solvents, water and decalin, played an important role in determining the product distribution. Besides benzene, cyclohexane was another major deoxygenated product when decalin was used as the sole solvent. In contrast, in the presence of a polar solvent, whether in the monophasic water system or in the biphasic

water-decalin system, benzene is the only deoxygenated product. In all three solvent systems, the oxygenated by-products, cyclohexanol and cyclohexanone, were presented. Benzene might be formed from the DDO of phenol by cleaving the $C_{sp^2}-O$ bond via hydrogenolysis, while an alternative pathway is through dehydration of cyclohexanol followed with dehydrogenation of cyclohexene, which may be promoted by Brønsted acids. For the Ru/5Nb₂O₅-5MC catalyst, the oxophilic sites of niobium, represented by incompletely coordinated Nb⁵⁺ cations (Lewis acid sites) near the perimeter of the Ru metal particles, could be converted to Brønsted acid sites as exposed to water. Furthermore, the Nb₂O₅-MC composites have a much higher acidity than Nb₂O₅ (Figure 4). It is very interesting that the presence of water may suppress the hydrogenation of benzene to cyclohexane in the biphasic solvent system.

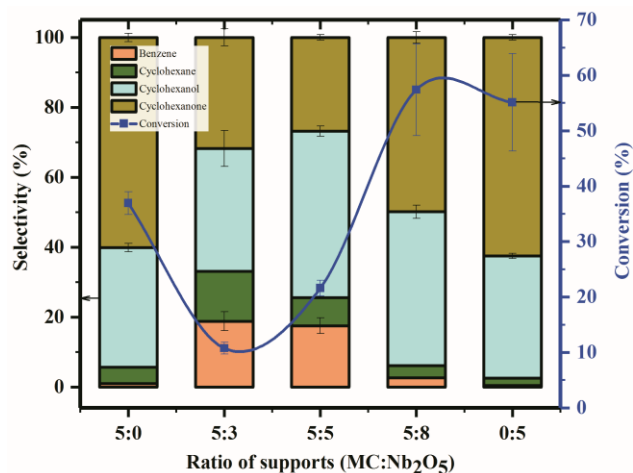


Fig. 7 Conversion, selectivity to benzene, cyclohexanol and cyclohexanone for the HDO of phenol at 200 °C and 6 bar H₂ for 4h over Ru/Nb₂O₅-MC catalyst with different ratio of Nb₂O₅ to MC supports.

The HDO activity of supported Ru catalysts on the Nb₂O₅, MC, and Nb₂O₅-MC composite supports were further examined at the different ratios of MC to Nb₂O₅ (ranging from 5:0 to 0:5) in the biphasic solvent system at a relatively low temperature (ca. 250 °C). As shown in Figure 7, the conversions of phenol over various catalysts are in the order of: Ru/8Nb₂O₅-5MC > Ru/Nb₂O₅ > Ru/MC > Ru/5Nb₂O₅-5MC > Ru/3Nb₂O₅-5MC. The conversions over the Ru on Nb₂O₅-MC composite support catalysts, except Ru/8Nb₂O₅-5MC, are lower than those over the Ru on Nb₂O₅ or MC single support catalysts. On the other hand, the selectivity to benzene over the Ru on Nb₂O₅-MC composite catalysts was significantly improved as the yield of benzene over the Ru catalyst on the single support (MC or Nb₂O₅) was negligible in the biphasic system. Especially, the selectivity to benzene over Ru supported on 3Nb₂O₅-5MC and 5Nb₂O₅-5MC composites were approximately five to six times higher compared to those over Ru/8Nb₂O₅-5MC with high content of Nb₂O₅. The reactions over the Ru catalysts with only the single support were more prone to produce cyclohexanol and cyclohexanone through the HYD pathway. However, the HDO of phenol did not occur over only


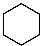
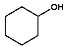
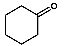
the catalyst supports without Ru (Table S4). It is worthwhile to notice that the hydrophilic-hydrophobic balance (the proportion of Nb₂O₅ and MC) of the Ru catalysts in the biphasic system plays a key role for tuning the selectivity to benzene from HDO of phenol. Here, the hydrophilic Nb₂O₅ species hold dual functions: the strong affinity to phenol, as well as the distinct capability of reducing the disassociation energy for C–O bonds.⁹ Moreover, the Ru nanoparticles were well dispersed on MC which possessed a hydrophobic character and high specific surface area (Table 1). The amphiphilic nature of the Nb₂O₅-MC composites makes these catalysts to be preferentially compartmented at the water/oil interface instead of dispersing in either bulk phase, which could stabilize the emulsion and thus enhance the mass transfer of molecules between the different phases (Figure S5). In addition, the biphasic catalytic process can facilitate the separation of hydrophobic molecules (such as benzene) from the aqueous phase, and thus convert those molecules selectively in only one of the liquid phases (i.e., phase-selectivity), simply based on differences in solubility.⁵⁸ The separation of the compounds into the decalin and water solvent layers with different polarities alleviates the fragment repolymerization. Therefore, high benzene yield can be obtained without the formation of chars. Therefore, the superior performance of the Ru/5Nb₂O₅-5MC catalyst for the HDO of phenol originates from a combination of the strong affinity to phenol, the reduction of the disassociation energy of the C_{aromatic}-OH bonds, the biphasic catalysis and the synergistic effect between Ru and Nb₂O₅-MC composite support, leading to the high phenol conversion and benzene selectivity.

3.2.2 Influence of the ratio of decalin/water in the biphasic catalytic process. To unravel the nature behind the high catalytic activity of the Ru/5Nb₂O₅-5MC catalyst for the HDO of phenol in the biphasic catalytic process, further studies were carried out to investigate the effect of the ratio of organic solvent to water. The as-formed Pickering emulsion (Figure S6) provides a high interfacial surface area where the catalytic reactions take place. Meanwhile, the Pickering emulsion enhances local hydrogen concentration near the interface because hydrogen has higher solubility in organic phase than in water.^{49,59} In the Pickering emulsion stabilized by Ru/5Nb₂O₅-5MC, the oil/water ratio is a crucial factor in determining the properties and states of emulsion droplets, which would further affect the catalytic performance of the emulsion. Therefore, it is reasonable that there exist a proper decalin/water ratio to obtain the highest yield of benzene, as shown in Table 2. The conversion of phenol occurred in either hydrophobic decalin or hydrophilic water, but in different manners. For instance, the HDO of phenol carried out in monophasic decalin did not produce benzene, while produced ~7.1% of benzene in monophasic water. However, the selectivity to benzene increased substantially in the decalin/water biphasic solvents and reached a maximum of 30.2% when the decalin/water volume ratio was 15:5. We ascribe the improvements to the “solvent cage effect”,^{60,61} which is that the phenol molecules are hemmed into a cage of solvent by the catalyst at the oil-water interface of the emulsion droplets. Since phenol is more soluble in water than in decalin, phenol was more concentrated in water-in-decalin (W/O) emulsion (Figure S6). These molecules in the solvent cage will collide with each other more frequently than the molecules in the bulk solvent. Accordingly, the HDO of phenol would be accelerated in the

W/O emulsions. Further decreasing the ratio of decalin to water led to a decrease in the selectivity of benzene, possibly due to the enlargement of the size of the emulsion droplets. Note that water is essential for the phenol HDO reaction to promote the production yield of benzene. Water can donate a proton to Lewis acid sites on

the Ru/Nb₂O₅-MC catalyst. The hydrolyzed protons from water and the pressurized H₂ gas may be involved in the removal of phenolic hydroxyl groups from the phenol molecules,⁶² which improves the removal of oxygen functionalities during the HDO reactions.

Table 2 The effect of volumetric ratio between decalin and water for the HDO of phenol over Ru/5Nb₂O₅-5MC catalyst

Entry	Decalin/water (mL/mL)	Conversion (wt. %)	Selectivity (C mol. %)			
						
1	20/0	100.0	0	100.0	0	0
2	15/5	100.0	30.2	0	64.5	5.3
3	10/10	99.8	24.7	2.3	68.2	4.8
4	5/15	99.9	20.0	12.3	64.7	3.0
5	0/20	99.9	7.1	7.0	83.0	3.0

Reaction conditions: 10 bar of hydrogen, 200 °C, 4 h, Ru/5Nb₂O₅-5MC catalyst.

3.2.3 Influence of hydrogen pressure. The effect of hydrogen pressure on the catalytic activity of Ru/5Nb₂O₅-5MC for the HDO of phenol is significant, as shown in Figure 8. Without H₂, phenol was not reacted at all. However, the Ru/5Nb₂O₅-5MC catalyst exhibited good catalytic activities for the HDO of phenol under the H₂ atmosphere at a mild temperature (200 °C). With the increase of the H₂ pressure from 2 to 10 bar, the conversion of phenol increased and reached 100% and correspondingly, the selectivity to benzene increased from ~10% to ~27.7%, when the H₂ pressure was greater than 10 bar. The yield of cyclohexanone is peaked at about 2 bar of H₂, and meanwhile the yield of cyclohexanol increases gradually with increasing the H₂ pressure. The results imply that cyclohexanone is an intermediate product from the conversion of phenol and is subsequently hydrogenated to form cyclohexanol. The saturation of benzene via hydrogenation to produce cyclohexane started as the H₂ pressure was over 10 bar and was completed at the H₂ pressure of 15 bar. On the other hand, however, the yield of cyclohexanol reached a maximum under 15 bar of H₂ and was kept unchanged with further increasing the H₂ pressure. Comparable results have been reported in the literature concerning on the effect of hydrogen pressure.^{10,29,63} These results suggested that the DDO pathway of converting phenol to benzene is preferred at low H₂ pressures while a higher H₂ pressure favors the generation of cyclohexane and cyclohexanol. Therefore, to enhance the yield of aromatics and reduce the consumption of H₂ in the HDO reaction, the H₂ pressure should be optimized.

3.2.4 Influence of reaction temperature. Figure 9 shows that the conversion of phenol and the selectivity to various products change significantly in the biphasic catalyst process with the increase of reaction temperature. When the reaction was carried out at a lower temperature range (160–200 °C), it was found that the highly efficient HDO of phenol was achieved over the Ru/5Nb₂O₅-5MC catalyst with a full conversion of phenol, and cyclohexanol was the main product and only a small amount of benzene, cyclohexane and cyclohexanone was formed. Especially, the benzene selectivity

reached a maximum value of 30.2% at 200 °C when the H₂ pressure was kept at 10 bar. Further increasing the reaction temperature led to a sharp increase of the cyclohexanone yield, while, at the same time, the yields of benzene and cyclohexanol decreased to a negligible level, which indicated the existence of the reversible reaction between cyclohexanone and cyclohexanol in this process. Higher reaction temperatures were favorable for the production of cyclohexanone. Interestingly, at the high temperatures range (> 200 °C), increasing the temperature led to a decrease in the conversion of phenol since the HDO of phenol is an exothermic reaction, which is thermodynamically unfavorable at high temperatures.

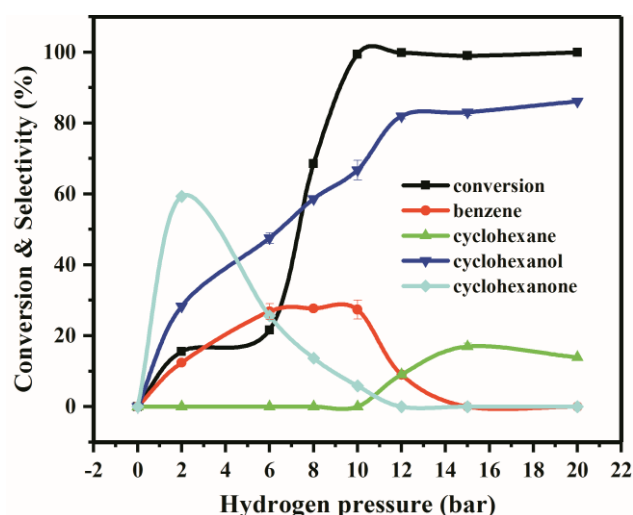


Fig. 8 Effect of the H₂ pressure. Reaction conditions: phenol (0.05 g), Ru/5Nb₂O₅-5MC (0.05 g), decalin/water = 10 mL/10 mL, 200 °C, 4 h.

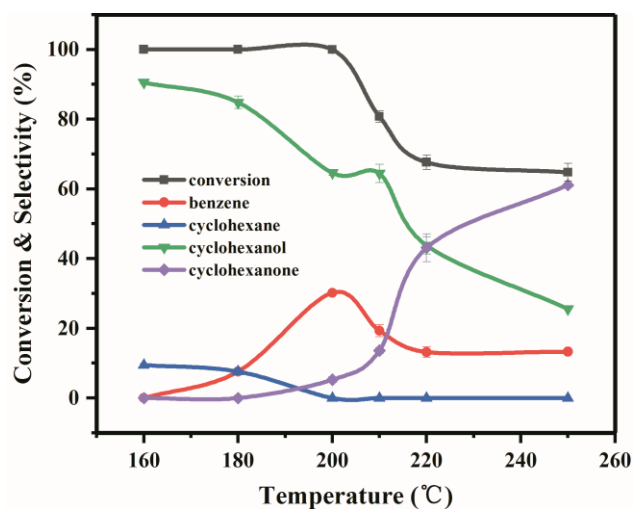


Fig. 9 Effect of reaction temperature on the catalytic activity of Ru/Nb₂O₅-MC for the HDO of phenol. Reaction conditions: phenol (0.05 g), Ru/5Nb₂O₅-5MC (0.05 g), 10 bar of hydrogen, decalin/water = 15 mL/5 mL, 4 h.

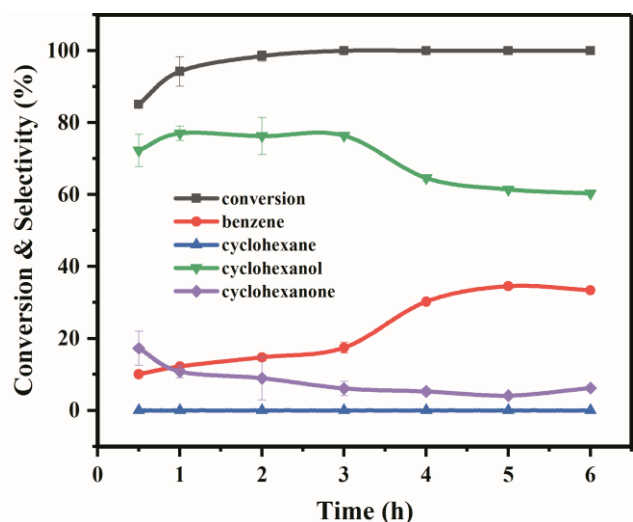


Fig. 10 Product distributions for HDO of phenol in biphasic system over Ru/Nb₂O₅-MC catalyst versus the time. Reaction conditions: phenol (0.05 g), Ru/5Nb₂O₅-5MC (0.05 g), 10 bar of hydrogen, decalin/water = 15 mL/5 mL, 200 °C.

3.2.5 Influence of reaction time. To further clarify the intrinsic reaction pathway, the kinetics behavior of the phenol over Ru/5Nb₂O₅-5MC was run for up to 6 hours in the water/decalin biphasic solvent (Figure 10). Along with extending the reaction time, the conversion of phenol kept increasing and finally reached the plateau at full conversion. The selectivity to benzene increased from ~10.1% at 0.5 h to ~30% at the full conversion of phenol, indicating that phenol was initially deoxygenated to benzene rapidly through the cleavage of C_{aromatic}-OH bond, implying that it is a fast step in the HDO of phenol possibly owing to the significant C_{aromatic}-OH bond activation on NbO_x species.⁶⁴ Meanwhile, the yield of cyclohexanone was peaked after about 0.5 h of the reaction time and then

decreased gradually, while the yield of cyclohexanol trended oppositely to that of cyclohexanone. The results imply that cyclohexanone is an intermediate product and can be converted to cyclohexanol over time. Interestingly, further prolonging the reaction time led to a decrease of the yield in cyclohexanol and an increase of the yield in benzene, which suggests the alternative pathway of producing benzene from cyclohexanol via dehydration and dehydrogenation (Table 3 and Scheme 1, route 1).¹²

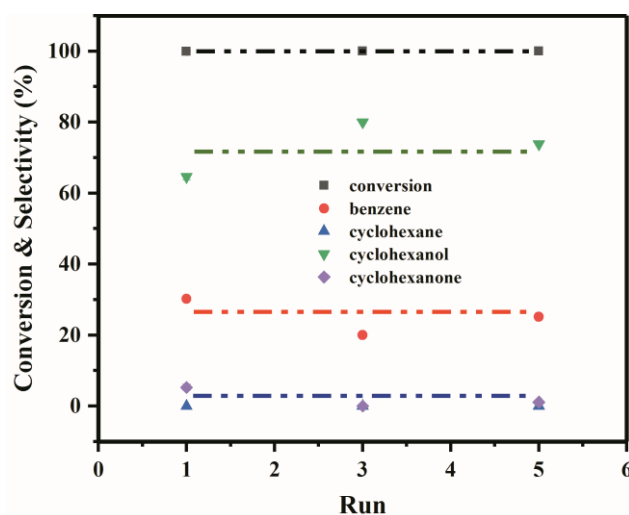
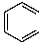
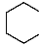
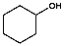
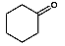
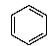
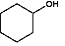
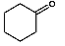


Fig. 11 Recycle of the catalyst. Reaction conditions: phenol (0.05 g), Ru/5Nb₂O₅-5MC (0.05 g), decalin/water = 15 mL/5 mL, 10 bar of hydrogen, 200 °C, 4 h.

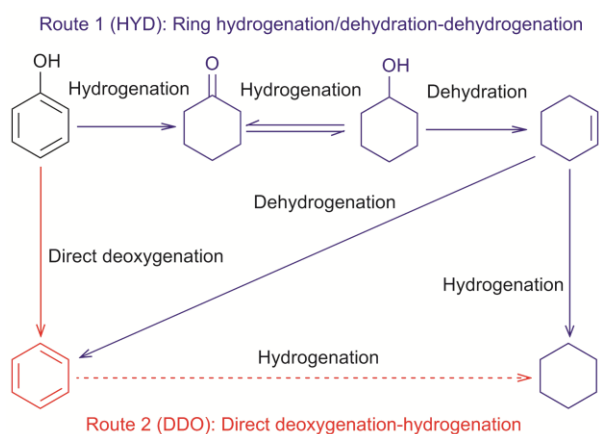
3.2.6 Recyclability of the catalysts. Catalyst stability and recyclability is important to evaluate heterogeneous catalysts. We tested the catalytic activity of the Ru/5Nb₂O₅-5MC catalyst in a typical biphasic catalytic process with successive runs and the results of conversions and yields are listed in Figure 11. As a result, the catalyst was successfully recycled for five times and it maintained a good activity, with only a slight decrease in the product yield. Interestingly, the catalyst can be partitioned into one phase so as to achieve the catalyst recycling via a simple phase separation without any loss in activity and selectivity.⁶⁵ Moreover, The XPS analysis of the spent catalyst showed that Ru^{x+} and Ru^{y+} in the catalyst were further reduced to Ru⁰ particles under the reductive reaction conditions (Figure 5).

3.2.7 Mechanism. Two different reaction pathways have been typically proposed in the literature for the HDO of phenol: (i) the direct deoxygenation (DDO) that involves the cleavage of the C(sp²)-O bond by hydrogenolysis and (ii) sequential hydrogenation (HYD) of the aromatic ring on metal sites followed by dehydration of cyclohexanol on acid sites.^{12,64,66} In order to clarify the reaction pathways of the HDO of phenol (especially, how the C-O bond was cleaved) over the Ru/5Nb₂O₅-5MC catalyst in the biphasic catalytic process, the probe reactions were performed using the possible intermediates or products, such as benzene, cyclohexanol and cyclohexanone, as the probe reactants (Table 3). We found that benzene was not liable to be converted to cyclohexane even under a

Table 3 HDO of the intermediate products over Ru/Nb₂O₅-MC catalyst in biTCP.

Entry	Feed materials	Conversion (wt. %)	Selectivity (C mol. %)			
						
1		13.10	–	100.0	0.0	0.0
2		7.13	15.6	84.4	–	0.0
3		97.16	1.1	4.8	94.1	–

Conditions: 200 °C, 10 bar of hydrogen, 4 h, 700 rpm.

**Scheme 1** Proposed reaction pathway of HDO of phenol in the biTCP over the Ru/Nb₂O₅-MC catalyst.

relatively high H₂ pressure (10 bar) as only ~13.1% of benzene was saturated by hydrogenation at 200 °C. This observation is in line with the literature report that hydrogenation of benzene to cyclohexene is thermodynamically unfavorable.⁶⁷ Moreover, the conversion of cyclohexanol was conducted to assess the relative concentration of surface Brønsted acid sites⁶⁸ on the supported Ru catalysts during the reaction. Table 3 shows that only a small amount of cyclohexanol was converted to cyclohexane and benzene through hydrogenation and dehydrogenation, respectively. In detail, cyclohexanol was dehydrated to form cyclohexene, and then underwent a hydrogenation step to produce cyclohexane, which is the dominant route, as the yield of cyclohexane from cyclohexanol was as high as ~84.4%. Contrarily, benzene was produced in a great disparity from the conversion of cyclohexanol and phenol, respectively, suggesting that in a typical biphasic catalytic process, benzene is produced primarily from the direct conversion of phenol via hydrogenolysis. Using cyclohexanone as feedstock, a large number of cyclohexanol and a small amount of cyclohexane are produced. These products could be formed by the following reaction pathways: the hydrogenation of cyclohexanone to cyclohexanol and dehydration of cyclohexanol to cyclohexene followed by a subsequent hydrogenation step to produce cyclohexane. Herein, we propose an overall reaction network of the HDO of phenol in the biphasic catalytic process, as shown in Scheme 1. The upper pathway (route

1) proceeds first through the catalytic hydrogenation (HYD) of phenol to form an unstable cyclohexene intermediate, followed by two potential pathways: (i) dehydrogenation to form benzene, or (ii) a hydrogenation step to cyclohexane. The lower pathway (route 2) is initiated by direct deoxygenation (DDO) of the C–O bond to produce benzene which then directly converted to cyclohexane slightly.

4. Conclusions

In summary, we have demonstrated an efficient catalytic process of converting phenol into benzene over the Ru/Nb₂O₅-MC catalysts in the biphasic decalin/water solvent systems. The HDO of phenol was promoted by a synergistic effect between the Ru nanoparticles catalyst and the Nb₂O₅-MC composite support, in which Ru catalyzes hydrogenation/dehydrogenation reactions while the Nb₂O₅-MC composite acidic sites adsorb the oxygenated compounds, activate the C_{aromatic}-OH bonds, and promote dehydration reactions. The tunable wettability of the Nb₂O₅-MC composite support was the key parameter for the formation of emulsions in the biphasic system. The presence of water in the biphasic catalytic process limits the saturation of benzene by hydrogenation and thus improves the selectivity towards benzene. The process conditions, including reaction temperature, hydrogen partial pressure, and reaction time, significantly affected the conversion of phenol and the selectivity to benzene. In general, higher temperatures, lower hydrogen partial pressures, and longer reaction time promoted the yield of benzene from phenol in the biphasic catalytic process. Under the optimum conditions (250 °C, 2 bar H₂), a full conversion of phenol and a high benzene selectivity of 80% were achieved over the Ru/5Nb₂O₅-5MC catalyst in the biphasic catalytic process. The probe reaction studies suggest that the formation of benzene is achieved mainly through the direct deoxygenation route. Overall, this biphasic catalytic process is excellent for phenol conversion, yielding a considerable amount of benzene under mild conditions with the low hydrogen consumption. The biphasic catalytic approach demonstrated in this research is expected to be further extended to transform lignin-derived phenolic compounds into aromatic compounds.

Conflicts of interest

There are no conflicts to declare.

Acknowledgements

This material is based on work supported by the National Science Foundation under grant no. CBET 1700482 (USA) and the National Natural Science Foundation of China (No. 21577025), the National Key Technology Support Program (No. 2015BAD15B06), the National Key Research and Development Program of China (No. 2017YFC0212205), and the International Cooperation Project of Shanghai Municipal Science and Technology Commission (No. 18230710700).

References

- 1 D. Verma, R. Insyani, H. S. Cahyadi, J. Park, S. M. Kim, J. M. Cho, J. W. Bae and J. Kim, *Green Chem.*, 2018, **20**, 3253–3270.
- 2 P. M. Mortensen, J. Grunwaldt, P. A. Jensen and A. D. Jensen, *ACS Catal.*, 2013, **3**, 1774–1785.
- 3 A. Corma Canos, S. Iborra, A. Velty, Avelino Corma, Sara Iborra, and Alexandra Velty, A. Corma, S. Iborra and A. Velty, *Chem. Rev.*, 2007, **107**, 2411–2502.
- 4 P. M. Mortensen, J. Grunwaldt, P. A. Jensen, K. G. Knudsen and A. D. Jensen, *Appl. Catal. A, Gen.*, 2011, **407**, 1–19.
- 5 C. Ju, M. Li, Y. Fang and T. Tan, *Green Chem.*, 2018, **20**, 4492–4499.
- 6 R. W. Gosselink, D. R. Stellwagen and J. H. Bitter, *Angew. Chemie - Int. Ed.*, 2013, **52**, 5089–5092.
- 7 J. He, C. Zhao and J. A. Lercher, *J. Am. Chem. Soc.*, 2012, **134**, 20768–20775.
- 8 S. Gillet, M. Agedo, L. Petitjean, A. R. C. Morais, A. M. Da Costa Lopes, R. M. Łukasik and P. T. Anastas, *Green Chem.*, 2017, **19**, 4200–4233.
- 9 Y. Shao, Q. Xia, L. Dong, X. Liu, X. Han, S. F. Parker, Y. Cheng, L. L. Daemen, A. J. Ramirez-Cuesta, S. Yang and Y. Wang, *Nat. Commun.*, 2017, **8**, 1–9.
- 10 R. C. Nelson, B. Baek, P. Ruiz, B. Goundie, A. Brooks, M. C. Wheeler, B. G. Frederick, L. C. Grabow and R. N. Austin, *ACS Catal.*, 2015, **5**, 6509–6523.
- 11 Y. Zeng, Z. Wang, W. Lin and W. Song, *Chem. Eng. J.*, 2017, **320**, 55–62.
- 12 I. T. Ghampson, C. Sepúlveda, A. B. Dongil, G. Pecchi, R. García, J. L. G. Fierro and N. Escalona, *Catal. Sci. Technol.*, 2016, **6**, 7289–7306.
- 13 H. Wang, J. Male and Y. Wang, *ACS Catal.*, 2013, **3**, 1047–1070.
- 14 W. S. Lee, Z. Wang, R. J. Wu and A. Bhan, *J. Catal.*, 2014, **319**, 44–53.
- 15 G. Wu, K. L. More, C. M. Johnston and P. Zelenay, *Science (80-)*, 2011, **332**, 443–448.
- 16 V. Molinari, C. Giordano, M. Antonietti and D. Esposito, *J. Am. Chem. Soc.*, 2014, **136**, 1758–1761.
- 17 S. Kusumoto and K. Nozaki, *Nat. Commun.*, 2015, **6**, 1–7.
- 18 J. Zakzeski, P. C. A. Bruijninx, A. L. Jongerius and B. M. Weckhuysen, *Chem. Rev.*, 2010, **110**, 3552–3599.
- 19 Y. K. Lugo-José, J. R. Monnier and C. T. Williams, *Appl. Catal. A Gen.*, 2014, **469**, 410–418.
- 20 M. B. Griffin, G. A. Ferguson, D. A. Ruddy, M. J. Bidy, G. T. Beckham and J. A. Schaidle, *ACS Catal.*, 2016, **6**, 2715–2727.
- 21 S. Boullosa-Eiras, R. Lødeng, H. Bergem, M. Stöcker, L. Hannevold and E. A. Blekkan, *Catal. Today*, 2014, **223**, 44–53.
- 22 A. Berenguer, T. M. Sankaranarayanan, G. Gómez, I. Moreno, J. M. Coronado, P. Pizarro and D. P. Serrano, *Green Chem.*, 2016, **18**, 1938–1951.
- 23 A. L. Jongerius, R. W. Gosselink, J. Dijkstra, J. H. Bitter, P. C. A. Bruijninx and B. M. Weckhuysen, *ChemCatChem*, 2013, **5**, 2964–2972.
- 24 I. T. Ghampson, C. Sepúlveda, R. Garcia, B. G. Frederick, M. C. Wheeler, N. Escalona and W. J. Desisto, *Appl. Catal. A, Gen.*, 2012, **413–414**, 78–84.
- 25 Q. Xia, Z. Chen, Y. Shao, X. Gong, H. Wang, X. Liu, S. F. Parker, X. Han, S. Yang and Y. Wang, *Nat. Commun.*, 2016, **7**, 1–10.
- 26 N. Cody, X. Zhou, B. Goundie, I. T. Ghampson, R. A. Pollock and Z. Ross, *Appl. Catal. A Gen.*, 2014, **477**, 64–74.
- 27 T. Omotoso, S. Boonyasuwat and S. P. Crossley, *Green Chem.*, 2014, **16**, 645–652.
- 28 Y. B. Huang, L. Yan, M. Y. Chen, Q. X. Guo and Y. Fu, *Green Chem.*, 2015, **17**, 3010–3017.
- 29 Z. Luo, Z. Zheng, Y. Wang, G. Sun, H. Jiang and C. Zhao, *Green Chem.*, 2016, **18**, 5845–5858.
- 30 A. G. Sergeev, J. D. Webb and J. F. Hartwig, *J. Am. Chem. Soc.*, 2012, **134**, 20226–20229.
- 31 Z. Luo, Y. Wang, M. He and C. Zhao, *Green Chem.*, 2016, **18**, 433–441.
- 32 X. Wang and R. Rinaldi, *Angew. Chemie - Int. Ed.*, 2013, **52**, 11499–11503.
- 33 S. Crossley, J. Faria, M. Shen and D. E. Resasco, *Science (80-)*, 2010, **327**, 68–72.
- 34 S. P. Teong, G. Yi, H. Zeng and Y. Zhang, *Green Chem.*, 2015, **17**, 3751–3755.
- 35 H. Liu, Z. Zhang, H. Yang, F. Cheng and Z. Du, *ChemSusChem*, 2014, **7**, 1888–1900.
- 36 B. P. Binks and S. O. Lumsdon, *Langmuir*, 2000, **16**, 8622–8631.
- 37 L. Wang and F. S. Xiao, *ChemCatChem*, 2014, **6**, 3048–3052.
- 38 M. Shen and D. E. Resasco, *Langmuir*, 2009, **25**, 10843–10851.
- 39 J. S. Yoon, J. W. Choi, D. J. Suh, K. Lee, H. Lee and J. M. Ha, *ChemCatChem*, 2015, **7**, 2669–2674.
- 40 M.-Y. Chen, Y.-B. Huang, H. Pang, X.-X. Liu and Y. Fu, *Green Chem.*, 2015, **17**, 1710–1717.
- 41 X. Yang, Y. Liang, X. Zhao, Y. Song, L. Hu, X. Wang, Z. Wang and J. Qiu, *RSC Adv.*, 2014, **4**, 31932.
- 42 X. Yang, T. Li, K. Tang, X. Zhou, M. Lu, W. L. Ounkham, S. M. Spain, B. J. Frost and H. Lin, *Green Chem.*, 2017, **19**, 3566–3573.
- 43 X. Yang, M. H. Uddin, X. Zhou, B. Neupane, G. C. Miller, C. J. Coronella, S. R. Poulson and H. Lin, *ACS Sustain. Chem. Eng.*, 2018, **6**, 10108–10119.
- 44 T. Li, S. S. G. Ong, J. Zhang, C. Jia, J. Sun, Y. Wang and H. Lin, *Catal. Today*, 2018, DOI: 10.1016/J.CATTOD.2018.11.052.
- 45 R. A. Kadir, R. A. Rani, A. S. Zoofakar, J. Z. Ou, M. Shafiei, W. Wlodarski and K. Kalantar-Zadeh, *Sensors Actuators, B Chem.*, 2014, **202**, 74–82.
- 46 T. Sreethawong, S. Ngamsinlapasathian, S. H. Lim and S. Yoshikawa, *Chem. Eng. J.*, 2013, **215–216**, 322–330.
- 47 R. Nava, B. Pawelec, P. Castaño, M. C. Álvarez-Galván, C. V. Loricera and J. L. G. Fierro, *Appl. Catal. B Environ.*, 2009, **92**, 154–167.

- 48 X. Zhao, L. Huang, S. Namuangruk, H. Hu, X. Hu, L. Shi and D. Zhang, *Catal. Sci. Technol.*, 2016, **6**, 5543–5553.
- 49 Z. Zhu, H. Tan, J. Wang, S. Yu and K. Zhou, *Green Chem.*, 2014, **16**, 2636.
- 50 U. E. S. Amjad, G. Gonçalves Lenzi, N. R. Camargo Fernandes-Machado and S. Specchia, *Catal. Today*, 2015, **257**, 122–130.
- 51 K. Qadir, S. M. Kim, H. Seo, B. S. Mun, F. A. Akgul, Z. Liu and J. Y. Park, *J. Phys. Chem. C*, 2013, **117**, 13108–13113.
- 52 L. L. Atanasoska, D. A. Cullen and R. T. Atanasoski, *J. Serbian Chem. Soc.*, 2013, **78**, 1993–2005.
- 53 N. Wang, W. Qian, W. Chu and F. Wei, *Catal. Sci. Technol.*, 2016, **6**, 3594–3605.
- 54 H. Huang, Q. Dai and X. Wang, *Appl. Catal. B Environ.*, 2014, **158–159**, 96–105.
- 55 M. Wang, H. Shi, D. M. Camaioni and J. A. Lercher, *Angew. Chemie - Int. Ed.*, 2017, **56**, 2110–2114.
- 56 D. J. Rensel, S. Rouvimov, M. E. Gin and J. C. Hicks, *J. Catal.*, 2013, **305**, 256–263.
- 57 B. P. Binks, J. Philip and J. A. Rodrigues, *Langmuir*, 2005, **21**, 3296–3302.
- 58 P. A. Zapata, J. Faria, M. P. Ruiz, R. E. Jentoft and D. E. Resasco, *J. Am. Chem. Soc.*, 2012, **134**, 8570–8578.
- 59 X. Yang, Y. Liang, Y. Cheng, W. Song, X. Wang, Z. Wang and J. Qiu, *Catal. Commun.*, 2014, **47**, 28–31.
- 60 C. Reichardt and T. Welton, *Solvents and Solvent Effects in Organic Chemistry*, 2014.
- 61 C. Li, H. Cai, B. Zhang, W. Li, G. Pei, T. Dai, A. Wang and T. Zhang, *Cuihua Xuebao/Chinese J. Catal.*, 2015, **36**, 1638–1646.
- 62 M. LR, G. Peng, R. Bechstein, F. Rieboldt and C. Farberow, *Science (80-.)*, 2012, **889**, 889–894.
- 63 T. Ngoc, Y. Park, I. Lee and C. Hyun, *Appl. Catal. A, Gen. J.*, 2017, **544**, 84–93.
- 64 T. Guo, Q. Xia, Y. Shao, X. Liu and Y. Wang, *Appl. Catal. A, Gen.*, 2017, **547**, 30–36.
- 65 M. Schmidt, T. Pogrzeba, L. Hohl, A. Weber, A. Kielholz, M. Kraume and R. Schomäcker, *Mol. Catal.*, 2017, **439**, 1–8.
- 66 P. M. De Souza, R. C. Rabelo-neto, L. E. P. Borges, G. Jacobs, B. H. Davis, T. Sooknoi, D. E. Resasco and F. B. Noronha, *ACS Catal.*, 2015, **5**, 1318–1329.
- 67 E. Shin and M. A. Keane, *Ind. Eng. Chem. Res.*, 2000, **39**, 883–892.
- 68 P. M. De Souza, R. C. Rabelo-neto, L. E. P. Borges, G. Jacobs, B. H. Davis, U. M. Graham, D. E. Resasco and F. B. Noronha, *ACS Catal.*, 2015, **5**, 7385–7398.